Accepted for publication in Journal of the American Ceramic Society lbnl report #45162

The Wulff Shape of Alumina: I. Modelling the Kinetics of Morphological Evolution

Mikito Kitayama,*,1,❖ Takayuki Narushima,*,1,✣ W. Craig Carter,*,2
Rowland M. Cannon, Jr.*,1 and Andreas M. Glaeser*,1

[1]Department of Materials Science and Mineral Engineering,
University of California, & Center for Advanced Materials
Lawrence Berkeley National Laboratory, Berkeley, CA 94720

[2]Department of Materials Science and Engineering
Massachusetts Institute of Technology
Cambridge, MA 02139

Abstract

The rate at which fully facetted nonequilibrium shaped particles and pores approach their equilibrium (Wulff) shape *via* surface diffusion was modelled, and calculations relevant to alumina were performed to guide experimental studies. The modelling focusses on 2-d features, and considers initial particle/pore shape, size, surface energy anisotropy, and temperature (surface diffusivity) as variables. The chemical potential differences driving the shape change are expressed in terms of facet-to-facet differences in weighted mean curvature. Two approaches to modelling the surface flux are taken. One linearizes the difference in the mean chemical potential of adjacent facets, and assumes the flux is proportional to this difference. The other approach treats the surface chemical potential as a continuous function of position, and relates the displacement rate of the surface to the divergence of the surface flux. When consistent values for the relevant materials parameters are used, the predictions of these two modelling approaches agree to within a factor of 1.5. As expected, the most important parameters affecting the evolution times are the cross-sectional area (volume in 3-d) and the temperature through its effect on the surface diffusivity. Pores of micron size are predicted to reach near-equilibrium shapes in reasonable times at temperatures as low as 1600°C. The detailed geometry of the initial nonequilibrium shape and the Wulff shape appear to have relatively minor effects on the times required to reach a near-equilibrium shape.

*Member, American Ceramic Society
❖Now at Synergy Ceramics Laboratory, Fine Ceramics Research Association, 1-1 Hirate-cho, Kita-ku, Nagoya 462 Japan
✣On leave from Tohoku University, Sendai, Japan

Introduction

The shape changes undergone by solid particles, and by precipitates and cavities (pores) within solids constitute an important element of microstructural evolution in materials. Such morphological changes are evident during sintering, and more generally, occur whenever materials are held at elevated temperatures for prolonged periods. The mass flows responsible for these shape changes can occur predominantly through the vapor phase, through the bulk, along a solid-vapor interface (a surface) or along a solid-solid interface (a grain boundary). The rate of shape change can be limited by the rate of mass arrival *via* gas, bulk, surface, or grain boundary diffusion. Alternatively, the shape change rate can be limited by the rate at which mass can be incorporated at a mass sink or can be released or supplied by a mass source. The general term surface-attachment-limited kinetics (sa1k) is used in this paper to refer to such situations, in which the rate of a nucleation step or of an attachment/detachment step limits the shape change rate.

Models treating a variety of diffusion-rate-limited shape changes in idealized materials with isotropic surface energies were developed during the 1950's and 1960's. These included treatments of surface (scratch) smoothing [1], grain boundary grooving [2], particle sintering [3-5], and Rayleigh instabilities of solid rods and cylindrical cavities in solids [6]. These models served two important roles. In cases where the relevant transport data were available, the models could be used in a predictive manner. In cases where transport data were absent, the experimental results could be evaluated using these models to provide needed transport data. Most of the surface diffusion data available for ceramic systems has been inferred from rates of morphological change assumed to be controlled by surface diffusion.

Subsequent treatments of the aforementioned processes have focussed on extending their range of applicability, and examining the behavior of less idealized systems. Accordingly, some efforts have focussed on evaluating the effects of higher-order (nonlinear) terms on the predictions of the models and improving the accuracy of predictions for more advanced stages of these processes [e.g., 7, 8]. Others have focussed on the effects of more complex initial or other boundary conditions on the predicted behavior [e.g., 9, 10]. In general, these analyses have retained the assumption of isotropic surface energy.

Other modelling efforts have focussed on incorporating the effects of surface energy anisotropy on morphological evolution. For a particle or cavity of fixed volume held at constant temperature, the driving force for shape changes is the associated reduction in the total surface energy. In many crystalline solids, the lowest energy form of a particle or cavity includes facets, and the equilibrium or Wulff shape can be fully facetted. The Wulff theorem prescribes that the equilibrium shape of such a particle or cavity is that for which

$$\frac{\gamma_1}{l_1} = \frac{\gamma_2}{l_2} = \frac{\gamma_3}{l_3} = \ldots = \frac{\gamma_i}{l_i} = \text{constant} \qquad (1)$$

where l_i is the physical distance from the center of mass of the crystal to the *i*th facet measured along a normal to the *i*th facet, and γ_i is the energy per unit area of the *i*th facet [11]. Surface energy anisotropy will alter the final state of a system, and influence the driving forces and kinetics of the processes that transform it from an initial nonequilibrium state [12, 13]. The appearance of facets can also lead to a change in the rate-controlling mechanism.

The influence of surface energy anisotropy and facetting on the energetics and kinetics of shape changes has become the topic of increasing attention. Bonzel, Mullins and their collaborators have examined the effect of surface energy anisotropy on scratch smoothing behavior, and have developed elegant new experimental methods and refined theoretical models [14-19]. Taylor, Cahn, Carter, and colleagues [20-22] have addressed a broad range of problems involving shape changes in facetted crystals, and have provided theoretical descriptions of shape changes controlled by both surface diffusion and by sa1k.

Within the past decade, methods that allow the introduction of large numbers of cavities of controlled size and shape into single crystal substrates of controlled surface orientation and their subsequent conversion to intragranular defects have been developed. These methods have been used examine the high-temperature properties of surfaces and interfaces in ceramics [23-33]. Since it is possible to generate defects with shapes that differ substantially from the equilibrium shape, arrays of such defects can be used as a vehicle for systematic investigation of the kinetics of shape evolution. Moreover, micron-sized pores can easily be produced by microlithographic methods, and it is expected that pores of this size

(or smaller) are necessary to reduce the equilibration time to reasonable levels [34-36]. Thus, *if* pores of such experimentally accessible sizes approach their equilibrium shape in reasonable times, then the Wulff shape (of a large number of cavities under prescribed conditions) can be determined.

For such small intragranular cavities, surface diffusion is expected to be the dominant diffusional process in alumina. Two treatments of the surface-diffusion-controlled shape evolution rate of fully facetted rodlike pores have recently been presented [34, 37]. For this 2-d case, at fixed temperature, the predicted times to equilibrate pores of fixed cross-sectional area and common initial shape in alumina differed by a factor of $\approx 10^3$. Errors in both models caused this large disparity.† Compounding this, different geometric parameters were used to track the evolution of the system, and thus, a direct comparison of the predictions was cumbersome.

This paper re-evaluates the two approaches to modelling surface-diffusion-controlled pore shape evolution, and isolates the effects of different modelling assumptions on the predicted evolution rates. A key finding is that when consistent values for the relevant materials parameters are used, these two modelling approaches yield predictions that agree to within a factor of 1.5. This close agreement has several important implications. The 2-d result suggests that if surface diffusion limits the evolution rate, it should be possible (with patience) to reach near-equilibrium shapes for micron-size pores that can readily be fabricated using microlithographic methods. It also suggests that the approximate method described in references [37, 38] can be extended from the 2-d cases, which can easily be treated using the exact method [34], to the more experimentally relevant 3-d cases where the exact method is extremely difficult to apply. This is the subject of a companion paper [39], in which the predictions of the 3-d model are compared to the results of model experiments assessing pore shape equilibration rates, and the role of ledge-producing defects (dislocations) on evolution rates are discussed. Collectively the results of these two studies proved useful in guiding the design of experiments aimed at determining the Wulff shape of doped and undoped aluminas. The results of the Wulff shape studies will be reported separately [40-42].

† The driving force formulation in reference [37] was incorrect. Even when this was corrected [38], and the same values of materials parameters were used, the disparity remained large. It was subsequently found that the predicted times in Figure 8 of reference [34] are inconsistent with the stated value of the surface diffusivity; this numerical error significantly impacts the interpretation of the experimental results presented in reference [34]. There is also an error in Eqn. 5 of reference [34]. Details are provided in the results section of this paper. A short note further detailing and correcting these errors is in preparation.

Background

Modelling the kinetics of shape change for fully facetted particles and cavities by surface diffusion involves several critical steps. These include formulating the driving force for shape changes, developing an equation to describe the surface flux, relating this flux to a change in particle shape, and solving the resulting differential equation that specifies the rate of shape change. In this section, we focus on presenting two different formulations of the driving force for the shape change. One assesses the net change of surface energy per mole of mass transferred from a receding facet to an advancing facet; this differential geometry approach defines a chemical potential difference. The second approach assesses the free energy change associated with surface formation per unit volume swept as a facet advances. This is the weighted mean curvature [20], and allows one to define the chemical potential on a facet-by-facet basis.

Feature Geometry

The discussion will focus on fully facetted *N*-sided rodlike particles or pore channels in a solid. The geometry of interest consists of an *N*-gon lying in the *x-y* plane that extends indefinitely in the *z*-direction, as illustrated in Figure 1. Vectors lying in the *x-y* plane extend from an origin 0, to *N* points, Q_1, Q_2, Q_3, …, Q_N. These *N* vectors have lengths l_1, l_2, l_3, … , l_v, … , l_N. Normals to these vectors passing through the points Q_1, Q_2, Q_3, … , Q_N define the facet planes. The edge lengths of the *N*-gon (the facet widths), denoted e_1, e_2, e_3, … , e_v, … , e_N depend upon the orientations and lengths of the *N* vectors, and are limited by intersections with other adjoining facets. The facets form a convex body enclosing a cross-sectional area A_{cs}. The volume per unit depth V' is A_{cs}•1.

Relationships for an Equilibrium-Shape Crystal

The procedure for determining the equilibrium shape of a 3-d facetted crystal can be found in standard reference texts [e.g., 43]. It involves minimizing the Helmholtz free energy of a body of constant volume and numbers of moles at constant temperature. Since only shape changes are allowed, the problem entails minimizing $\Phi = \sum_{j=1}^{N} \gamma_j A_j$ at constant volume where A_j is the area of facet *j*, and can be solved using the method of Lagrange multipliers. For the fully facetted 2-d crystals/cavities of interest here, V' is held constant, and a similar minimization procedure leads to a set of *N* equations of the form

$$\sum_{j=1}^{N} \frac{\partial A_j}{\partial l_\nu}\left(\gamma_j - \eta\, l_j\right) = 0 \qquad \text{for } \nu = 1,2,\ldots,N \tag{2}$$

where A_j is the area of facet *j* per unit depth, and η is a Lagrange multiplier. One possible solution is

$$\frac{\gamma_1}{l_1} = \frac{\gamma_2}{l_2} = \ldots = \frac{\gamma_N}{l_N} = \eta \tag{3}$$

which is the 2-d analog of Eqn. (1).

The procedures for defining the chemical potential of a crystal having the Wulff shape are also available in standard texts [e.g., 43]. For a facetted crystal having the Wulff shape, the chemical potential exceeds that of an infinite size crystal by an amount that is proportional to γ_j / l_j

$$\mu_{l_1} = \mu_\circ + \frac{\overline{V}\gamma_1}{l_1} = \mu_\circ + \frac{\overline{V}\gamma_2}{l_2} = \ldots = \mu_\circ + \frac{\overline{V}\gamma_N}{l_N} \tag{4}$$

where $\mu_\circ$ is the bulk chemical potential, and $\overline{V}$ is the molar volume. Thus, for a particle with the Wulff shape, the ratio γ_j / l_j plays the same role as $\gamma\kappa$ in an isotropic system, where κ is the curvature.

Relationships for a Non-Equilibrium-Shape Crystal

Eqn. (4) is valid *only* for a crystal having the equilibrium shape; for the Wulff shape the chemical potential is the same on all facets.[*] A more general formulation of the chemical potential beneath a facetted surface, applicable to non-equilibrium shape crystals and cavities, was presented by Herring [12]. The effect of an infinitesimal displacement of a plane surface parallel to itself is considered, and leads to a definition of an area-average potential. The further extension of this concept has led to the weighted mean curvature as a means of defining the chemical potential of each facet. We will define the weighted mean curvature (*wmc*) to be *the limit of the rate of change of surface energy with respect to the volume swept as the volume swept goes to zero*.[❖] Following the discussion of Taylor [20] with the current sign convention, for a segment S_i of a polygonal surface, the *wmc* is given by,

[*] If Eqn. (4) is used to specify the chemical potential of mass on a facet of a *nonequilibrium* shape particle, the facet-to-facet chemical potential differences that are implied would lead to pathological flows, *i.e.*, such definitions of the potential make the Wulff shape an unstable equilibrium state, and are not pertinent for nonequilibrium cases.

[❖] Taylor [20] originally defined the weighted mean curvature, *wmc*, as the negative of this quantity. In subsequent papers by Cahn and Taylor [21, 22], and in this paper, the sign convention is reversed to parallel the sign convention normally used for κ.

$$wmc(S_i) = \frac{1}{Length(S_i)} \sum_{j \neq i} \delta_{ij} f_{ij} \tag{5}$$

where δ_{ij} is +1 for a convex (positive) crystal, and -1 for a concave (negative) crystal. The term f_{ij} is

$$f_{ij} = \frac{\gamma_j - c_{ij}\gamma_i}{\sqrt{1 - c_{ij}^2}} \tag{6}$$

where

$$c_{ij} = \vec{n}_i \cdot \vec{n}_j = \left|\vec{n}_i\right|\left|\vec{n}_j\right| \cdot \cos\theta \tag{7}$$

and $\vec{n}_i$ and $\vec{n}_j$ are the unit normals to surfaces *i* and *j*, and θ is the angle between them.

The chemical potential associated with facet *j* depends on the *wmc* of the facet, and is given by

$$\mu_j = \mu_\circ + \bar{V}(wmc)_j \tag{8}$$

The *wmc* reduces to a form involving γ_j / l_j when a crystal or cavity has the equilibrium shape.

The Driving Force for Shape Changes

In general, there are two approaches to formulating the driving force for shape changes. The first computes the free energy change associated with the transfer of mass from one facet to the other, determines the free energy change per mole of mass transferred, and thus defines a chemical potential difference, $\Delta\mu$. The second approach employs the concept of weighted mean curvature to specify the chemical potential on each facet, *e.g.*, μ_1 and μ_2, and evaluates the difference in these chemical potentials, $\mu_1 - \mu_2$, to define a driving force. In this section we apply both of these methods to the case of a stretched square and a stretched hexagon. The resulting driving force expressions are used in the modelling to calculate the shape change rates for these two geometries.

Stretched Square

For the rectangular cross-section illustrated in Figure 2a, the condition of constant volume per unit depth implies $A_{cs} = 4l_1l_2 = constant$. Letting Φ represent the surface energy per unit depth of crystal in the

z-direction, shape changes that conserve volume and involve normal displacements of the facets produce a differential surface energy change per unit depth of crystal given by

$$\left(d\Phi\right)_{total} = (4 \bullet 1)\left[\gamma_1 dl_2 + \gamma_2 dl_1\right] = (4 \bullet 1)\left[\gamma_2 - \gamma_1 \frac{l_2}{l_1}\right] dl_1 \tag{9}$$

This expression equals zero when the Wulff condition, Eqn. (3), is satisfied. When l_2 exceeds the equilibrium value, the term in brackets is negative, and $d\Phi$ is negative when dl_1 is positive.

The transfer of *dn* moles from a single surface of area A_2 per unit depth and energy γ_2 to a single surface of area A_1 per unit depth and energy γ_1, produces a differential surface energy change

$$\left(d\Phi\right)_{2\to 1} = (2 \bullet 1)\left[\gamma_2 - \gamma_1 \frac{l_2}{l_1}\right] dl_1 \tag{10}$$

The volume per unit depth swept due to the displacement of facet 1 by an amount dl_1, dV_1, can be related to the number of moles transferred, *dn*, and the molar volume, $\overline{V}$, as follows

$$dV_1 \approx 2l_2 \bullet 1 \bullet dl_1 = \overline{V} dn \quad \Longrightarrow \quad dl_1 = \frac{\overline{V} dn}{2l_2 \bullet 1} \tag{11}$$

Inserting this into Eqn. (10) and rearranging, the differential energy change is

$$\left(d\Phi\right)_{2\to 1} = \overline{V}\left(\frac{\gamma_2}{l_2} - \frac{\gamma_1}{l_1}\right) dn \tag{12}$$

The ratio of the free energy change and number of moles transferred is a chemical potential difference, and thus, we obtain

$$\left(\frac{d\Phi}{dn}\right)_{2\to 1} = \Delta\mu_{2\to 1} = \mu_1 - \mu_2 = \overline{V}\left(\frac{\gamma_2}{l_2} - \frac{\gamma_1}{l_1}\right) \tag{13}$$

For the stretched square geometry, one can infer that the term involving $\overline{V}\gamma_2 / l_2$ is associated with μ_1 and the term involving $\overline{V}\gamma_1 / l_1$ is associated with μ_2. When the geometry is more complex, it is not always obvious which of the γ_i / l_i terms is associated with which facet. Only $\Delta\mu_{2\to 1}$ is clearly specified.

A treatment of the driving force in terms of weighted mean curvature explicitly defines the (mean) chemical potential of each facet. For the simple geometries under discussion here, the *wmc* values can easily be assessed by examining the surface energy change per unit volume swept graphically. Figures 3a and 3b show the surface area changes as a result of displacements δl_1 and δl_2. Assessing the surface energy changes and volume swept, it follows that the *wmc* of facets 1 and 2, wmc_1 and wmc_2, respectively, are

$$wmc_1 = \frac{2\gamma_2(\delta l_1 \bullet 1)}{(2l_2 \bullet 1)\bullet \delta l_1} = \frac{\gamma_2}{l_2} \qquad wmc_2 = \frac{2\gamma_1(\delta l_2 \bullet 1)}{(2l_1 \bullet 1)\bullet \delta l_2} = \frac{\gamma_1}{l_1} \tag{14}$$

Applying Eqn. (8), the chemical potentials on facets 1 and 2, μ_1 and μ_2, respectively, are

$$\mu_1 = \mu_\circ + \overline{V}\left(\frac{\gamma_2}{l_2}\right) \qquad \mu_2 = \mu_\circ + \overline{V}\left(\frac{\gamma_1}{l_1}\right) \tag{15}$$

Stretched Hexagon

The geometry of the stretched hexagon, Figure 4, is slightly more complex than that of the stretched square, and this has led to differences in the description of the geometry, and in the choice of metric used to characterize the approach to equilibrium. For example, A_{cs} can be defined in three ways

$$A_{cs} = 2l_1e_1 + l_1e_2 = l_1e_1 + 2l_2e_2 = 4e_2l_2 - e_2l_1 \tag{16}$$

where

$$e_1 = \frac{2}{\sqrt{3}}(2l_2 - l_1) \qquad e_2 = \frac{2}{\sqrt{3}}l_1 \tag{17}$$

The constant A_{cs} constraint leads to the following relationship between dl_1 and dl_2

$$dl_2 = -\frac{2l_2 - l_1}{2l_1}dl_1 \tag{18}$$

The surface energy per unit depth of crystal, Φ, can be written,

$$\Phi = \sum_{i=1}^{N}\gamma_i A_i = \gamma_1 2A_1 + \gamma_2 4A_2 = 2\gamma_1 e_1 \bullet 1 + 4\gamma_2 e_2 \bullet 1 \tag{19}$$

If we assume that the shape changes involve normal displacements of facets and maintain symmetry, the differential surface energy change of unit depth of crystal in response to a shape change at constant V' will be given by

$$\left(d\Phi\right)_{total} = \left[2 \bullet \gamma_1 \left(-\frac{4}{\sqrt{3}} \frac{l_2}{l_1} dl_1\right) + 4 \bullet \gamma_2 \left(\frac{2}{\sqrt{3}} dl_1\right)\right] \bullet 1 = \frac{8}{\sqrt{3}} \left[\gamma_2 - \gamma_1 \frac{l_2}{l_1}\right] dl_1 \bullet 1 \tag{20}$$

When $\gamma_1 / l_1 = \gamma_2 / l_2$, $d\Phi$ equals zero as it should. When l_2 exceeds the equilibrium value, the term in brackets is negative, and $d\Phi$ is negative when dl_1 is positive.

The differential change in surface energy when one transfers *dn* moles from the two identical flanking surfaces of area A_2 per unit depth and energy γ_2 to a single surface of area A_1 per unit depth and energy γ_1 is

$$\left(d\Phi\right)_{2\to 1} = \left[1 \bullet \gamma_1 \left(-\frac{4}{\sqrt{3}} \frac{l_2}{l_1} dl_1\right) + 2 \bullet \gamma_2 \left(\frac{2}{\sqrt{3}} dl_1\right)\right] \bullet 1 = \frac{4}{\sqrt{3}} \left[\gamma_2 - \gamma_1 \frac{l_2}{l_1}\right] dl_1 \bullet 1 \tag{21}$$

The volume per unit depth swept due to the displacement of facet 1 by an amount dl_1, dV_1, can again be related to the number of moles transferred, *dn*, and the molar volume, $\overline{V}$. For this geometry

$$dV_1 \approx e_1 \bullet 1 \bullet dl_1 = \overline{V} dn \quad \Rightarrow \quad dl_1 = \frac{\overline{V} dn}{e_1 \bullet 1} \tag{22}$$

As a result,

$$\left(\frac{d\Phi}{dn}\right)_{2\to 1} = \Delta\mu_{2\to 1} = \mu_1 - \mu_2 = \frac{4}{\sqrt{3}} \left(\gamma_2 - \gamma_1 \frac{l_2}{l_1}\right) \frac{\overline{V}}{e_1 \bullet 1} \bullet 1 = 2\overline{V} \left(\frac{l_1 \gamma_2 - l_2 \gamma_1}{l_1 \left(2l_2 - l_1\right)}\right) \tag{23}$$

The numerator goes to zero when $\gamma_1 / l_1 = \gamma_2 / l_2$. The chemical potential difference goes to infinity when $2l_2 = l_1$; geometrically, when this condition is satisfied, the length of facet 1, e_1, goes to zero, as shown by Eqn. (17).

The same result can be obtained by evaluating the difference in *wmc* of facets 1 and 2. Figures 4a and 4b illustrate the surface area and surface energy changes as a result of displacements δl_1 and δl_2,

respectively. For facet 1, the surface area per unit depth is $e_1 \bullet 1$, and the volume swept by a displacement δl_1 is $e_1 \bullet 1 \bullet \delta l_1$. The displacement of facet 1 by δl_1 increases the area of each of the inclined facets of energy γ_2 by an amount $\left(2/\sqrt{3}\right)\delta l_1 \bullet 1$, resulting in a surface energy change, $\left(4/\sqrt{3}\right)\gamma_2 \delta l_1 \bullet 1$. In addition, the displacement decreases the length of facet 1, by an amount $\left(1/\sqrt{3}\right)\delta l_1 \bullet 1$ at each end, resulting in a surface energy decrease of $\left(2/\sqrt{3}\right)\gamma_1 \delta l_1 \bullet 1$. It follows that wmc_1, is

$$wmc_1 = \left(\frac{4}{\sqrt{3}}\gamma_2 \delta l_1 \bullet 1 - \frac{2}{\sqrt{3}}\gamma_1 \delta l_1 \bullet 1\right) \Big/ \frac{2}{\sqrt{3}}\left(2l_2 - l_1\right)\delta l_1 \bullet 1 = \frac{2\gamma_2 - \gamma_1}{2l_2 - l_1} \tag{24}$$

At equilibrium, this ratio is equivalent to $\left(\gamma_1 / l_1\right)$. The displacement of each inclined facet by an amount δl_2 extends facet 1 by an amount $\left(2/\sqrt{3}\right)\delta l_2 \bullet 1$, and thus, the energy increase is $\left(2/\sqrt{3}\right)\gamma_1 \delta l_2 \bullet 1$. The volume swept is $\approx e_2 \bullet 1 \bullet \delta l_2$, and thus,

$$wmc_2 = \left(\frac{2}{\sqrt{3}}\delta l_2 \bullet 1\right)\gamma_1 \Big/ \left(\frac{2}{\sqrt{3}} l_1 \bullet 1\right)\delta l_2 = \frac{\gamma_1}{l_1} \tag{25}$$

which is equal to $\left(\gamma_2 / l_2\right)$ at equilibrium. The driving force for transfer of mass from facet 2 to facet 1 is

$$\Delta\mu_{2\to 1} = \mu_1 - \mu_2 = \overline{V}\left[\left(\frac{2\gamma_2 - \gamma_1}{2l_2 - l_1}\right) - \left(\frac{\gamma_1}{l_1}\right)\right] = 2\overline{V}\left(\frac{l_1\gamma_2 - l_2\gamma_1}{l_1\left(2l_2 - l_1\right)}\right) \tag{26}$$

For both the stretched square and the stretched hexagon, the chemical potential on a facet *i* is affected by the energy of the adjacent facets, γ_j. The pairing of μ_i with the ratio γ_i / l_i obscures this, and results in relationships only valid when the crystal or cavity has the equilibrium shape.

Modelling

When a facetted crystal or a facetted cavity has the equilibrium shape, the *wmc* and the chemical potential will be constant, and there is no driving force for mass transfer and shape changes. In contrast, when the shape deviates from the Wulff shape, the *wmc* and the chemical potential will vary from facet to facet on the particle or pore surface. This spatial variation in the chemical potential creates a driving force for mass transfer that allows the system to approach the equilibrium shape, albeit asymptotically.

For mass transport controlled by surface diffusion, the surface flux, J_s, can be related to the gradient in the chemical potential at the surface. Fick's first law of diffusion for the surface flux (in atoms/m^2•s) can be written as

$$J_s = -\frac{D_s}{\bar{V}\mathrm{k}T} \bullet \frac{d\mu}{dx} \tag{27}$$

where D_s is the surface diffusion coefficient, $\bar{V}$ is the molar volume, k is Boltzmann's constant, and T is absolute temperature. The local rate of mass accumulation, and thus the surface displacement rate, hinges on the gradient in the flux. The normal velocity of a surface, V_n can thus be expressed as

$$V_n = -\frac{dJ_s}{dx}\delta_s\bar{V} = \frac{\delta_s D_s}{\mathrm{k}T} \bullet \left(\frac{d^2\mu}{dx^2}\right) \tag{28}$$

where δ_s is the width over which diffusion is enhanced.

If the chemical potential on the facet of a nonequilibrium shape crystal were assumed constant on the entire facet, then chemical potential discontinuities would exist at facet edges. Yu and Hackney [44] formulated the positional dependence of the surface potential on a facet in a nonequilibrium shape crystal, using an approach suggested by Herring [12]. When facets undergo uniform normal displacements the rate of mass deposition or removal must be uniform on each facet. The gradient or divergence of the flux must be constant on each facet, and it follows from Eqn. (28) that $\nabla^2\mu$ must be constant on each facet. Yu and Hackney [44] treated the case of a stretched square evolving by surface diffusion. Generalized procedures were developed independently by Carter *et al.*, and presented in references [22] and [34]. If position on facets 1 and 2 in the direction of flow is measured by the variables *x* and y, respectively, then for the 2-d problems of interest, a possible general solution to the chemical potential variation across facets 1 and 2 takes the form

$$\mu_s^{(1)}(x) = c_1x^2 + c_2x + c_3 \qquad \mu_s^{(2)}(y) = d_1y^2 + d_2y + d_3 \tag{29}$$

where c_1, c_2, and c_3 and d_1, d_2, and d_3 are constants whose values are chosen to match the boundary conditions. The *average* value of the chemical potential on facet *i* is equated to that dictated by the *wmc* of

the facet, Eqn. (8). The potential and the potential gradient must be continuous at the facet edge. Symmetry considerations provide additional boundary conditions.

For the stretched square, taking $x = 0$ and $y = 0$ as the midpoints of facets 1 and 2, respectively,

$$\begin{aligned}\mu_s^{(1)}(x) &= \frac{3}{2}\overline{V}\left[\frac{(\gamma_1/l_1)-(\gamma_2/l_2)}{l_2(l_2+l_1)}\right]\left(x^2-\frac{l_2^2}{3}\right)+\mu_\circ+\overline{V}\left(\frac{\gamma_2}{l_2}\right)\\ \mu_s^{(2)}(y) &= -\frac{3}{2}\overline{V}\left[\frac{(\gamma_1/l_1)-(\gamma_2/l_2)}{l_1(l_2+l_1)}\right]\left(y^2-\frac{l_1^2}{3}\right)+\mu_\circ+\overline{V}\left(\frac{\gamma_1}{l_1}\right)\end{aligned} \tag{30}$$

The same general method can be applied to the stretched hexagon, however, in that case, the potential on facet 2 is asymmetric about the midpoint; the gradient of the surface potential equals zero at the junction point of the two inclined facets located distance l_2 from the origin. These equations can then be used in conjunction with Eqn. (28) to prescribe an exact value for the displacement rate of the facets.

This approach is relatively simple to apply to 2-d problems, but satisfying the boundary conditions becomes very difficult when the diffusion problem is three-dimensional. Thus, a simpler approach to estimating the rate of facet displacement, one that is more easily applied to 3-d problems was pursued.

Regardless of the form of the chemical potential gradient on a facet, the total mass arrival rate for a facet is the sum of the mass flow rates at the facet edges. These flow rates are dictated by the potential gradients at the facet edges. If we implicitly assume that the deposition rate is uniform on the facet, the problem reduces to one of estimating the gradients at the facet edges. Kitayama [45] has approximated the gradient at the facet edge as the difference in the mean potentials on the adjoining facets divided by an "effective diffusion distance". As a result, Eqn. (27) is applied to the edge, and modified to be

$$\left(J_s\right)_{2\to1} = -\frac{D_s}{\overline{V}\mathrm{k}T}\bullet\frac{\Delta\overline{\mu}_{2\to1}}{\Delta x_{2\to1}} \tag{31}$$

where $\Delta\overline{\mu}_{2\to1} = \overline{\mu}_1 - \overline{\mu}_2$ represents the difference in mean potential, and $\Delta x_{2\to1}$ is the effective diffusion distance. The mean chemical potentials, $\overline{\mu}_1$ and $\overline{\mu}_2$ are calculated using Eqn. (8). For the stretched square, the potential will be either a minimum or maximum at the facet centers, and either a maximum or minimum at the facet edges, depending upon whether the facet acts a mass sink or a mass source. If the

center-to-edge variation of potential with position is linearized, and Eqn. (8) is used to define the mean potential, then the potential is at its mean value for facets 1 and 2 at distances $l_1/2$ and $l_2/2$ from the corner, respectively. The sum of these distances is used to scale the potential difference, and is referred to as an effective diffusion distance. (For the stretched hexagon, $\Delta x_{2\to1}$ is $(e_1/4)+(e_2/2)$.)

The two approaches are compared in Figure 5 for a stretched square. The parabolic potentials are drawn, and compared with the facet-edge gradient that results when $\Delta x_{2\to1}$ is set equal to $(l_1 + l_2)/2$. Note that the slopes are similar, and that the quality of the agreement hinges on the choice of $\Delta x_{2\to1}$. For the given choice, the parabolic potential leads to a potential gradient at the facet edge that is 1.5× that for the "linearized" gradient. As a result, the times predicted by the linearized gradient method for a given change of shape will be 1.5× the value obtained by the more exact method. Similar comparisons for the case of a stretched hexagon, with the effective diffusion distance taken to be $(e_1/4)+(e_2/2)$ lead to a factor of 1.5 difference in the edge fluxes, with the continuous potential again yielding the higher evolution rate.

The calculations of the displacement rates for facet 1 for both the stretched square and the stretched hexagon involve the following steps. The infinitesimal volume change of a single facet of type 1, dV_1, during an infinitesimal time interval *dt* is expressed as

$$dV_1 = A_1 dl_1 = J_s \bullet \delta_s \bullet L \bullet \Omega \bullet dt \tag{32}$$

where A_1 is the area per unit depth of facet 1, δ_s is taken here to be equal to $\Omega^{1/3}$ where Ω is the atomic volume, and L is the total common or shared edge length between the interacting facets. The product $\delta_s \bullet L$ represents the area through which diffusion is occurring. This equation can be rearranged and combined with Eqn. (31) to yield the following differential equation for the displacement rate of facet 1

$$\frac{dl_1}{dt} = \frac{J_s \bullet \delta_s \bullet L \bullet \Omega}{A_1} = -\frac{D_s \Omega^{4/3}}{\bar{V} \mathrm{k} T} \bullet \frac{L}{A_1} \bullet \frac{\Delta \bar{\mu}_{2\to1}}{\Delta x_{2\to1}} \tag{33}$$

For the stretched square, with $\Delta \bar{\mu}_{2\to1}$ given by Eqn. (13), $\Delta x_{2\to1}$ set equal to $(l_1 + l_2)/2$, and l_2 set equal to $A_{cs}/4l_1$, the potential gradient can be written as

$$\left(\frac{\Delta\overline{\mu}}{\Delta x}\right)_{StrSq} = \frac{2\overline{V}\left(\frac{\gamma_2}{l_2}-\frac{\gamma_1}{l_1}\right)}{(l_1+l_2)} = \frac{8\overline{V}}{A_{cs}}\left(\frac{\gamma_2 \bullet 4l_1^2 - \gamma_1 \bullet A_{cs}}{4l_1^2 + A_{cs}}\right) \tag{34}$$

The potential gradient at the corner ($x = l_2$ and $y = -l_1$) implied by Eqn. (30) is 1.5× this value. For unit depth of the stretched square, taking $A_1 = 2l_2 \bullet 1$, $L = 2$, and using Eqn. (34), Eqn. (33) takes the form

$$\left(\frac{dl_1}{dt}\right)_{StrSq} = -\frac{32D_s\Omega^{4/3}}{kT} \bullet \frac{1}{A_{cs}^2} \bullet \frac{\gamma_2 \bullet 4l_1^3 - \gamma_1 \bullet l_1 A_{cs}}{4l_1^2 + A_{cs}} \tag{35}$$

Letting $R_{eq} = (\gamma_2 / \gamma_1)$ this equation can be re-expressed as

$$\left(\frac{dl_1}{dt}\right)_{StrSq} = -\frac{32D_s\Omega^{4/3}\gamma_1}{kT} \bullet \frac{1}{A_{cs}^2} \bullet \frac{l_1\left(R_{eq} \bullet 4l_1^2 - A_{cs}\right)}{4l_1^2 + A_{cs}} \tag{36}$$

Solving for *dt* and integrating leads to

$$(t-t_0)_{StrSq} = \left(\frac{kT}{D_s\Omega^{4/3}\gamma_1}\right)\left[\frac{A_{cs}^2}{32} \bullet \ln\left(\frac{l_1^{(t)}}{l_1^{(t_0)}}\right) - \frac{A_{cs}^2\left(1+R_{eq}\right)}{64R_{eq}} \bullet \ln\left(\frac{A_{cs} - 4(l_1^{(t)})^2 R_{eq}}{A_{cs} - 4(l_1^{(t_0)})^2 R_{eq}}\right)\right] \tag{37}$$

where $l_1^{(t_0)}$ is the value of l_1 at time t_0 and $l_1^{(t)}$ is the value of l_1 at time *t*. Since A_{cs} is homogeneous of degree 2, a uniform enlargement of the particle by a factor λ increases A_{cs} by a factor λ^2, and thus, the evolution time *t* scales with λ^4 as would be expected from the Herring scaling laws [46].

For the case of the stretched hexagon, $\Delta\overline{\mu}_{2\to1}$ is given by Eqn. (26), and the effective diffusion distance is $(e_1 / 4) + (e_2 / 2)$. Using Eqn. (17), the potential gradient can be written as

$$\left(\frac{\Delta\overline{\mu}}{\Delta x}\right)_{StrHex} = \frac{2\sqrt{3}\overline{V}}{(2l_2 + l_1)}\left(\frac{2\gamma_2 - \gamma_1}{2l_2 - l_1} - \frac{\gamma_1}{l_1}\right) \tag{38}$$

If we solve Eqn. (29) for the stretched hexagon, and evaluate the potential gradient at the corner we again find that it is 1.5× that obtained with a linearized potential. For a segment of crystal of unit depth, taking $A_1 = e_1 \bullet 1$, $L = 2$, using Eqn. (17) to re-express e_1, and Eqn. (16) to eliminate l_2, Eqn. (33) takes the form

$$\left(\frac{dl_1}{dt}\right)_{StrHex} = -\frac{96 D_s \Omega^{4/3}}{kT}\left(\frac{l_1\left[2l_1^2(4\gamma_2-\gamma_1)-\sqrt{3}A_{cs}\gamma_1\right]}{\left(\sqrt{3}A_{cs}+6l_1^2\right)\left(\sqrt{3}A_{cs}-2l_1^2\right)^2}\right) \tag{39}$$

With $R_{eq} = (\gamma_2 / \gamma_1)$, the integrated form of this expression can be written as

$$\begin{aligned}(t-t_0)_{StrHex} = \left(\frac{kT}{D_s\Omega^{4/3}\gamma_1}\right)\Bigg[&\frac{A_{cs}(5R_{eq}-2)}{8\sqrt{3}(4R_{eq}-1)^2}\left((l_1^{(t)})^2-(l_1^{(t_0)})^2\right)-\frac{\left((l_1^{(t)})^4-(l_1^{(t_0)})^4\right)}{32(4R_{eq}-1)}\\ &+\frac{A_{cs}^2}{32}\bullet\ln\left(\frac{l_1^{(t)}}{l_1^{(t_0)}}\right)-\frac{A_{cs}^2(2R_{eq}-1)^2(2R_{eq}+1)}{8(4R_{eq}-1)^3}\bullet\ln\left(\frac{\sqrt{3}A_{cs}+2(l_1^{(t)})^2-8(l_1^{(t)})^2R_{eq}}{\sqrt{3}A_{cs}+2(l_1^{(t_0)})^2-8(l_1^{(t_0)})^2R_{eq}}\right)\Bigg]\end{aligned} \tag{40}$$

The predicted times are a factor of 1.5 greater than those predicted for the parabolic potential.

Results

In this section we provide the results of three sets of calculations performed using values of materials parameters specific to aluminum oxide. These calculations examine the effect of 1) crystal or cavity size and shape, 2) temperature, and 3) the surface energy anisotropy on shape relaxation kinetics.

Effect of Crystal (Cavity) Volume and Shape on Relaxation Rates

The results of the modelling for both the stretched square and stretched hexagon geometry were used to calculate aspect ratio-time trajectories appropriate to alumina. For this purpose, the temperature was fixed at 1600°C, and an "average" value of the surface diffusivity D_s of 1.82×10^{-11} m^2/s was assumed. The relevant volume Ω was taken to be 2.11×10^{-29} m^3 [47], and the surface thickness δ_s was assumed to be of the order of $\Omega^{1/3}$. The surface energies, γ_1 and γ_2, were assumed to be equal and 1 J/m^2. The initial value of R_a (=w/d) was taken to be 15. Figure 6 plots the times required to reduce the aspect ratio R_a from 15 to the indicated values of R_a for both a stretched hexagon and a stretched square of fixed cross-sectional area, A_{cs} = 10^{-11} m^2. Aspect ratio–time trajectories for both the linearized and parabolic potentials are shown. The curves terminate when the value of R_a reaches 1.01 times its equilibrium value R_{eq}. The anneal

time required for intermediate changes in R_a, *e.g.*, from 10 to 5, is determined by assessing the difference in anneal time corresponding to these values of R_a.

Since the time to reach a given value of R_a from a common initial value is proportional to A_{cs}^2, the results predict that at 1600°C, features with a cross-sectional area of the order of 1 μm × 1 μm should reach values of R_a of 1.01•R_{eq} in 8 h or less. Using the values for D_s (10^{-10} m^2/s) and Ω (6.6×10^{-29} m^3) assumed by Choi *et al.* [34], the predicted relaxation times would be reduced by a factor ≈25. Submicron-sized features are not necessary to achieve near-equilibrium shapes at this temperature. Similar size scaling of the results in Figure 6 indicates that pores of the size examined by Choi *et al.* [34] ($A_{cs} \leq 10^{-13}$ m^2) should reach near-equilibrium shapes within only a few minutes at 1600°C if surface diffusion were rate-limiting. The relaxation kinetics suggested by Figure 8 in reference [34] imply that ≈50 h anneals would be required for shape equilibration of cavities with $A_{cs} = 10^{-13}$ m^2; this result is clearly inconsistent with the stated values of materials parameters.*

A comparison of the evolution kinetics of the stretched square and the stretched hexagon suggest that the relaxation rates are not particularly sensitive to the details of the crystal or cavity shape. This suggests that the more global geometric parameters such as the w/d ratio and the cross sectional area, that define the shape and volume are the key variables, and an approximate shape can be used to provide reasonable estimates of the evolution rate. At least in systems like alumina, where the uncertainty in the diffusivity is quite large, the details of the facet structure are not critical for kinetic modelling.

It is also the case that the details of the potential gradient have only a minor effect on the predicted evolution rates. The displacement rate of a facet hinges on the volume arrival rate, and this is dictated by the potential gradient at the facet edge. For reasonable choices of the effective diffusion distance, the potential gradient predicted using the difference in the mean potentials is close to that obtained when a parabolic potential is assumed. For both the stretched square and stretched hexagon, the linearized gradient

* The numerical error reflected in Figure 8 also impacts the interpretation of the experimental observations in reference [34]. The persistence of non-equilibrium shapes in such small facetted cavities suggests that in the absence of ledge-producing defects such as dislocations, the evolution rates are extremely sluggish, and not controlled by surface diffusion. Experimental results presented in the companion paper [39] also support this viewpoint. Recent calculations by Mullins and Rohrer [48] suggest that the barrier to the nucleation of new facet layers is extremely large for facets above a limiting size of ≈1 nm, making particles/cavities without alternative sources of ledges (dislocations) unable to adjust their shape.

and parabolic potential yield results that differ by only a factor of 1.5. This close agreement suggests that the linearized approach can be used to provide reasonable estimates in 3-d problems where solutions that are based on a continuously varying potential on the surface are more difficult to obtain.

Effect of Temperature

The time to reach a particular state, or to produce a particular shape change scales inversely with the diffusion coefficient. In assessing the surface diffusion data available for alumina, there is considerable scatter both in the magnitude of the diffusivity at fixed temperature, and in the apparent activation energy.◆ For the present purposes, an average value for the surface diffusivity is assumed, and the temperature dependence of the average surface diffusivity is calculated using:

$$D_s = D_\circ \exp^{(-Q_s/RT)} = 2360 \bullet \exp^{(-506000/RT)} \quad (m^2/s) \tag{41}$$

with the activation energy Q_s given in joules/degree•mole.

To illustrate the effect of temperature, the results for the two treatments of the stretched hexagon are compared in Figure 7. An initial R_a value of 15 is assumed, and A_{cs} is set equal to 10^{-11} m^2. Three temperatures are considered, 1600°C, 1800°C, and 2000°C. The predictions indicate that although a particle or pore of order a few microns in size would not equilibrate in an experimentally accessible time at 1600°C, such a feature is expected to reach $R_a \approx 1.01 \bullet R_{eq}$ in approximately one day at 1800°C. At the higher temperatures, an even broader size range of features becomes accessible, and it may be possible to examine scaling law behavior directly.

Effect of Surface Energy Anisotropy

In modelling the temporal evolution of particle and pore shapes, the possibility that different crystal faces would have different surface energies was incorporated. Previously, in considering the effects of size, shape and temperature, the two energies, γ_1 and γ_2, were set equal. Under these conditions, R_{eq} is unity for the stretched square. To examine the effects of surface energy anisotropy, two sets of calculations were performed for the stretched square. In both, the temperature was fixed at 1600°C, and A_{cs} was set

◆ In the scratch smoothing study of Bennison and Harmer [47], an error was made in converting previously reported values of D_S to the $\delta_S D_S$ format and units of m^3/s. Prior data is a factor of 100 too high in their Figure 1. When this error is corrected, the data obtained in their study agrees much more closely with average values in prior work.

equal to 10^{-11} m^2. A range of R_{eq} values, from 0.5 to 2.0, was then considered. In one calculation, the value of γ_1 is held fixed at 1 J/m^2, and changes in R_{eq} are accommodated by changing the value of γ_2; in this case, the average surface energy of the equilibrium shape crystal increases as R_{eq} increases. The results of this calculation are shown in Figure 8a. In the second calculation, the values of *both* γ_1 and γ_2 are adjusted to accommodate the change in R_{eq}, but in a way that maintains the *average* surface energy of the equilibrium shape crystal constant at 1 J/m^2. The results of this calculation are presented in Figure 8b. In both figures, the curves terminate when R_a reaches $1.01 \bullet R_{eq}$.

When the effect of varying R_{eq} is assessed, one concludes that the details of the anisotropy have only a minor influence on the time required to reach the near-equilibrium shape. When the average value of the surface energy is allowed to vary, Figure 8a, a factor of four change in R_{eq} results in only a factor ≈ 2 change in the time at which R_a reaches $1.01 \bullet R_{eq}$. When $R_a \geq 3$, the predicted times to reach a given R_a value vary by less than or equal to a factor of ≈ 1.5. When the average value of γ is held constant, the times at which R_a reaches $1.01 \bullet R_{eq}$ differ by only a few percent. In this case, when $R_a \geq 3$, the times required to achieve the associated shapes differ more substantially, varying by a factor of up to ≈ 3. Nonetheless, the results imply that if measured values of R_a are interpreted using a model that assumes the surface energies of all facets are equal, this assumption would introduce less than a $2\times$ error into the inferred value of D_s. Since measurements of relative surface energies in metallic systems [49-52], and recent measurements of relative surface energies in undoped [34, 40, 45] and doped aluminas [41, 42, 45] suggest that actual variations in γ are much smaller than considered in the calculation, such variations are not likely to be a major source of error in estimates of diffusivities. In contrast, unrecognized changes in the rate-limiting transport process from diffusion to sa1k, and assessment of morphology changes that involve growth or decay of perturbations on a stable facet *can* lead to significant errors in estimates of the surface diffusivity.

Summary and Conclusions

Models have been developed that allow calculations of the times required to adjust the shape of facetted rodlike particles and facetted pore channels by surface diffusion. The modelling has used

differential geometry and weighted mean curvature based descriptions of the driving force. Two different methods of describing the potential gradients driving the surface flux have been presented and compared. The method based on a continuously varying potential is more rigorous, but unfortunately also more difficult to apply to 3-d problems. It was thus of interest to determine the magnitude of the errors that arise when simpler approximations of the driving force, approximations that are more easily applied to 3-d problems, are used in modelling the behavior.

The results suggest that the crystal/cavity size and the temperature, through its influence on the surface diffusivity, are the key factors influencing the rate of pore shape evolution. The initial shapes considered in the modelling deviate significantly from the Wulff shape. Under these conditions, although the details of the feature shape, the formulation of the chemical potential gradient, and variations in the details of the surface energy anisotropy do influence the evolution times, the changes owing to these factors tend to be small, of the order of a factor of three or less. As a result, the general features of the evolution are not affected significantly by the subtleties of the initial shape, approximate treatments of the potential gradient, or the ultimate Wulff shape.

Significant simplifications have been made in the modelling. The surface diffusivity is assumed to be isotropic; differing diffusivities on adjoining facets introduce a discontinuity in the potential gradient at the facet edge [44]. The analysis does not address the nucleation of new facets, merely the displacement of those originally present. Perhaps most importantly it implicitly assumes that shape relaxation in fully facetted systems can be surface diffusion limited, and thus, that a sufficiently high ledge density exists. A reassessment of the experimental results of Choi *et al.* [34] suggests this may not be valid. The role of the atomistic structure of the surfaces undergoing displacements and the role of ledges in crystal growth was first discussed in the work of Burton, Cabrera and Frank [53] and similar issues relevant to shape equilibration constitute the focal point of analyses by Ozdemir and Zangwill [54], Bullard and Searcy [55] and Mullins and Rohrer [48].

The most compelling assessment of the importance of surface structure on the evolution of a facetted crystal or pore would be obtained by comparing experimental observations with modelling results. The close agreement between the linearized gradient and parabolic potential based models has encouraged

efforts to extend the former approach to the 3-d geometries that can be generated using microfabrication methods. Isolated feature with simple nonequilibrium shapes offer several important experimental advantages over the 2-d feature geometries treated in this paper, notably the absence of complications due to Rayleigh instabilities. The extension of the linearized-gradient approach to shape evolution of isolated nonequilibrium shape pores, and the results of a parallel experimental study are presented in a companion paper [39]. It will be demonstrated that a wide range of evolution behavior is encountered for cavities of identical volume and initial aspect ratio but differing crystallographic orientation. The results suggest that in many of these cases, consideration of surface attachment limited kinetics, and ledge availability is essential.

Acknowledgements

This work was supported by the Director, Office of Science, Office of Basic Energy Sciences, of the U.S. Department of Energy under Contract No. DE-AC03-76SF00098. Professor Narushima was on leave from Tohoku University at the time this manuscript was being developed, and acknowledges support from the Japan Ministry of Education, Science, Sports and Culture under Contract No. 9-Young Scientists-15. The authors thank Robert Marks for his careful review of the manuscript, and helpful suggestions. We also thank Professors Rohrer and Mullins for providing us with an advance copy of their modelling of patch nucleation rates on the surfaces of fully facetted particles and cavities.

References:

1. W. W. Mullins, "Flattening of a Nearly Plane Solid Surface due to Capillarity," *J. Appl. Phys.*, 30, [1], 77-83 (1959).

2. W. W. Mullins, "Theory of Thermal Grooving," *J. Appl. Phys.*, 28, [3], 333-39 (1957).

3. G. C. Kuczynski, "Self-Diffusion in Sintering of Metallic Particles," *Trans. A.I.M.E.*, 185, [2], 169-78 (1949).

4. W. D. Kingery and M. Berg, "Study of the Initial Stages of Sintering of Solids by Viscous Flow, Evaporation-Condensation, and Self-Diffusion," *J. Appl. Phys.*, 26, [10], 1205-12 (1955).

5. R. L. Coble, "Sintering Crystalline Solids. I. Intermediate and Final Stage Diffusion Models," *J. Appl. Phys.*, 32, [5], 787-92 (1961).

6. F. A. Nichols and W. W. Mullins, "Surface (Interface) and Volume-Diffusion Contributions to Morphological Changes Driven by Capillarity," *Trans. A.I.M.E.*, 233, [10], 1840-48 (1965).

7. R. F. Sekerka and T. F. Marinis, "Dynamics of Morphological Change during Solid-Solid Transformations," pp. 67-84 in Solid → Solid Phase Transformations, edited by H. I. Aaronson, D. E. Laughlin, R. F. Sekerka and C. M. Wayman, The Metallurgical Society of AIME, New York, (1982).

8. W. M. Robertson, "Grain-Boundary Grooving by Surface Diffusion for Finite Surface Slopes," *J. Appl. Phys.*, 42, [1], 463-67 (1971).

9. W. S. Coblenz, J. M. Dynys, R. M. Cannon, Jr., and R. L. Coble, "Initial Stage Solid-State Sintering Models: A Critical Analysis and Assessment," pp. 141-57 in Sintering Processes, G. C. Kuczynski, Editor, Plenum Press, NY, (1980).

References: (*cont.*)

10. J-H. Choy, S. A. Hackney and J. K. Lee, "Nonlinear stability analysis of the diffusional spheroidization of rods," *J. Appl. Phys.*, 77, [11], 5647-54 (1995).

11. G. Wulff, "Zur Frage der Geschwindigkeit des Wachstums und der Auflösung der Krystallflachen," *Z. Krist.*, 34, 449-530 (1901).

12. C. Herring, "Surface Tension as a Motivation for Sintering," pp. 143-79 in The Physics of Powder Metallurgy, W. E. Kingston, Ed. New York: McGraw-Hill, 1951

13. A. D. Brailsford and N. A. Gjostein, "Influence of surface energy anisotropy on morphological changes occurring by surface diffusion," *J. Appl. Phys.*, 46, [6], 2390-97 (1975).

14. H. P. Bonzel, E. Preuss and B. Steffen, "Periodic Surface Profiles Under the Influence of Anisotropic Surface Energy: A Steady-State Solution," *Surf. Sci.*, 145, [1], 20-32 (1984).

15. H. P. Bonzel, E. Preuss and B. Steffen, "The Dynamical Behavior of Periodic Surface Profiles on Metals Under the Influence of Anisotropic Surface Energy," *J. Appl. Phys. A* (*Solids and Surfaces)*, 35, [1], 1-8 (1984).

16. U. Breuer and H. P. Bonzel, "Morphology of Periodic Surface Profiles on Au Single Crystals and the Anisotropy of the Surface Free Energy of Au," *Surf. Sci.*, 273, [1], 219-36 (1992).

17. S. Surnev, B. Voigtländer, H. P. Bonzel, and W. W. Mullins, "Anisotropic profile decay on perturbed Au(111) vicinal surfaces," *Surf. Sci.*, 360, [1], 242-48 (1996).

18. H. P. Bonzel, and W. W. Mullins, "Smoothing of perturbed vicinal surfaces," *Surf. Sci.*, 350, [1], 285-300 (1996).

19. C. Duport, A. Chame, W. W. Mullins and J. Villain, "Decay of Grooves Cut in a Surface with Singular Orientation when the Neighboring Orientations are Unstable," *J. Phys. I France*, 6, 1095-1125 (1996).

References: (*cont.*)

20. J. E. Taylor, "Overview No. 98 II – Mean Curvature and Weighted Mean Curvature," *Acta Metall. Mater.*, 40, [7], 1475-85 (1992).

21. J. W. Cahn and J. E. Taylor, "Surface motion by surface diffusion," *Acta Metall. Mater.*, 42, [4] 1045-63 (1994).

22. W. C. Carter, A. R. Roosen, J. W. Cahn and J. E. Taylor, "Shape Evolution by Surface Diffusion and Surface Attachment Limited Kinetics on Completely Facetted Surfaces," *Acta Metall. Mater.*, 43, [12], 4309-4323 (1995).

23. J. Rödel and A. M. Glaeser, "Microdesigned Interfaces: New Opportunities for Materials Science," *Yogyo Kyokai Shi*, 99, [4], 251-65 (1991).

24. J. Rödel and A. M. Glaeser, "High-Temperature Healing of Lithographically Introduced Cracks in Sapphire," *J. Am. Ceram. Soc.*, 73, [3], 592-601 (1990).

25. J. D. Powers and A. M. Glaeser, "High-Temperature Healing of Cracklike Flaws in Mg- and Ca-Ion-Implanted Sapphire," *J. Am. Ceram. Soc.*, 75, [9], 2547-58 (1992).

26. J. D. Powers and A. M. Glaeser, "High-Temperature Healing of Cracklike Flaws in Titanium Ion-Implanted Sapphire," *J. Am. Ceram. Soc.*, 76, [9], 2225-34 (1993).

27. L. Kulinsky, J. D. Powers and A. M. Glaeser, "Morphological Evolution of Pre-perturbed Pore Channels in Sapphire," *Acta Mater.*, 44, [10], 4115-30 (1996).

28. J. S. Stölken and A. M. Glaeser, "The Morphological Evolution of Cylindrical Rods with Anisotropic Surface Free Energy *via* Surface Diffusion," *Scripta Metall. et Mater.*, 27, [4], 449-54 (1992).

References: (*cont.*)

29. A. M. Glaeser, "A New Approach to Investigating Surface Transport in Ceramics," pp. 117-36 in Mass and Charge Transport in Ceramics, K. Koumoto, L. M. Sheppard and H. Matsubara, Eds., *Ceram. Trans.*, 71, (1996).

30. J. Rödel and A. M. Glaeser, "Pore Drag and Pore-Boundary Separation in Alumina," *J. Am. Ceram. Soc.*, 73 [11] 3302-3312 (1990).

31. J. Rödel and A. M. Glaeser, "Anisotropy of Grain Growth in Alumina," *J. Am. Ceram. Soc.*, 73, [11], 3292-301 (1990).

32. J. D. Powers and A. M. Glaeser, "Titanium Effects on Sintering and Grain Boundary Mobility of Alumina," *Ceram. Eng. Sci. Proc.*, 18, [4], 617-23 (1997).

33. J. Rödel and A. M. Glaeser, "A Technique for Investigating the Elimination and Coarsening of Model Pore Arrays," *Mater. Lett.*, 6, [10], 351-55 (1988).

34. J. Choi, D. Kim, B. J. Hockey, S. M. Wiederhorn, C. A. Handwerker, J. E. Blendell, W. C. Carter, and A. R. Roosen, "The Equilibrium Shape of Internal Cavities in Sapphire," *J. Am. Ceram. Soc.*, 80, [1], 62-68 (1997).

35. R. Kern, "The Equilibrium Form of a Crystal," pp. 92-98 in Morphology of Crystals, Part A: Fundamentals, Ichiro Sunagawa, Editor, Terra Scientific Publishing Co., Tokyo, Japan (1987).

36. R. S. Nelson, D. J. Mazey, and R. S. Barnes, "The Thermal Equilibrium Shape and Size of Holes in Solids," *Phil. Mag.*, 11, 91-111 (1965).

37. M. Kitayama and A. M. Glaeser, "The Energetics and Kinetics of Pore Shape Evolution in Alumina," *Key Eng. Mater.*, 159-160, 193-204 (1999).

References: (*cont.*)

38. M. Kitayama and A. M. Glaeser, "The Kinetics of Pore Shape Evolution in Alumina," *J. Mater. Synth. Proc.*, 6, [3], 161-7 (1998).

39. M. Kitayama, T. Narushima and A. M. Glaeser, "The Wulff Shape of Alumina: II. Experimental Measurements of Pore Shape Evolution," *this volume.*

40. M. Kitayama and A. M. Glaeser, "The Wulff Shape of Alumina: III. Undoped Alumina," *in preparation.*

41. M. Kitayama and A. M. Glaeser, "The Wulff Shape of Alumina: IV. Ti(IV)-Doped Alumina," *in preparation.*

42. M. Kitayama and A. M. Glaeser, "The Wulff Shape of Alumina: V. Mg, Ca, and Ti(III)-Doped Alumina," *in preparation.*

43. C. H. P. Lupis, Chemical Thermodynamics of Materials, pp. 368-73, North-Holland, New York, NY, (1983).

44. S. H. Yu and S. A. Hackney, "On the shape change of a nonequilibrium faceted microcrystal," *Scripta Metall. Mater.*, 24, [11], 2077-82 (1990).

45. M. Kitayama, "The Wulff Shape of Doped and Undoped Sapphire," Ph.D. thesis, Department of Materials Science and Mineral Engineering, University of California, (December 1996).

46. C. Herring, "Effect of Change of Scale on Sintering Phenomena," *J. Appl. Phys.*, 21, [4], 301-03 (1950).

47. S. J. Bennison and M. P. Harmer, "Effect of Magnesia Solute on Surface Diffusion in Sapphire and the Role of Magnesia in the Sintering of Alumina," *J. Am. Ceram. Soc.*, 73, [4], 833-37 (1990).

References: (*cont.*)

48. W. W. Mullins and G. S. Rohrer, "Nucleation Barrier for Volume-Conserving Shape Changes of Faceted Crystals," *unpublished research*, (1999).

49. B. E. Sundquist, "A Direct Determination of the Anisotropy of the Surface Free Energy of Solid, Silver, Copper, Nickel, and Alpha and Gamma Iron," *Acta Metall.*, 12, [1], 67-86 (1964).

50. W. L. Winterbottom and N. A. Gjostein, "Determination of the Anisotropy of Surface Energy of Metals-II: Experimental γ-Plot of Gold," *Acta Metall.*, 14, [9], 1041-52 (1966).

51. M. McLean, "Determination of the Surface Energy of Copper as a Function of Crystallographic Orientation and Temperature," *Acta Metall.*, 19, [4], 387-93 (1971).

52. J. C. Heyraud and J. J. Métois, "Equilibrium Shape and Temperature; Lead on Graphite," *Surf. Sci.*, 128, 334-42 (1983).

53. W. K. Burton, N. Cabrera, and F. C. Frank, "The Growth of Crystals and the Equilibrium Structure of Their Surfaces," *Phil. Trans. Royal Soc. London*, 243, [866], 299-358 (1951).

54. M. Ozdemir and A. Zangwill, "Morphological equilibration of a facetted crystal," *Phys. Rev. B (Condensed Matter)*, 45, [7], 3718-29 (1992).

55. J. W. Bullard and A. W. Searcy, "Equilibria and kinetics of mass transport between crystal facets: a comparison of two models," *Acta Mater.*, 47, [10], 3057-61 (1999).

Figure Captions:

Figure 1 Parameters in a geometric description of a facetted solid rod or a facetted pore channel.

Figure 2 Illustration of the two geometries considered, and parameters used in the modelling. The geometry in (a) is referred to in the text as a stretched square, while that in (b) is termed a stretched hexagon.

Figure 3 Illustration of the surface area and surface energy changes associated with the morphological evolution of a stretched square. When these surface energy changes are divided by the volume swept, the *wmc* of the displaced facets is determined.

Figure 4a Illustration of the surface area and surface energy changes associated with the morphological evolution of a stretched hexagon. When the surface energy changes caused by the displacement of facet 1 are added and then divided by the volume swept, the *wmc* of facet 1 is determined.

Figure 4b Illustration of the surface area and surface energy changes associated with the morphological evolution of a stretched hexagon. The *wmc* of facet 2 is determined to be γ_1/l_1.

Figure 5 Comparison of the potential gradients at the edge of a stretched square when a parabolic potential (*pp*) is assumed, and when the mean chemical potential difference between adjacent facets is linearized (*lp*).

Figure 6 Comparison of the predicted time dependencies of the aspect ratio at 1600°C for stretched squares and stretched hexagons of fixed size.

Figure 7 Plot of the predicted effect of temperature on the shape equilibration kinetics of a stretched hexagon.

Figure 8 Predicted effect of surface energy anisotropy on the shape equilibration kinetics of a stretched square. In (b), the values of *both* γ_1 and γ_2 are adjusted to accommodate the change in R_{eq}, but the *average* surface energy of the equilibrium shape crystal is maintained constant at 1 J/m^2.

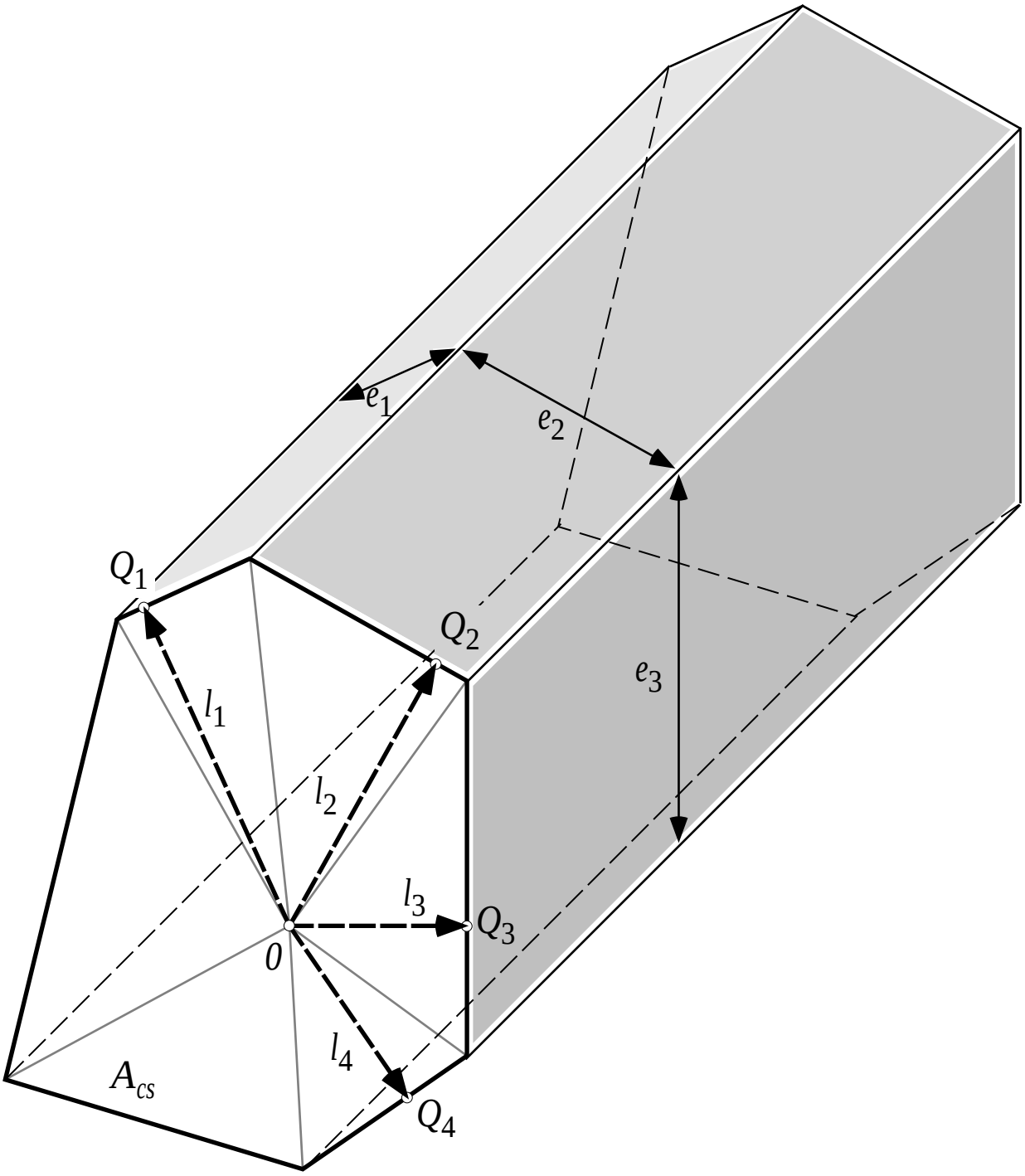

Figure 1 Parameters in a geometric description of a facetted solid rod or a facetted pore channel.